

Published in final edited form as:

Biochim Biophys Acta Bioenerg. 2018 September 01; 1859(9): 734–741. doi:10.1016/j.bbabi.2018.06.001.

How inter-subunit contacts in the membrane domain of complex I affect proton transfer energetics

Andrea Di Luca[#], Max E. Mühlbauer[#], Patricia Saura, Ville R.I. Kaila^{*}

Department Chemie, Technische Universität München, Lichtenbergstr. 4, Garching, D-85747, Germany

[#] These authors contributed equally to this work.

Abstract

The respiratory complex I is a redox-driven proton pump that employs the free energy released from quinone reduction to pump protons across its complete ca. 200 Å wide membrane domain. Despite recently resolved structures and molecular simulations, the exact mechanism for the proton transport process remains unclear. Here we combine large-scale molecular simulations with quantum chemical density functional theory (DFT) models to study how contacts between neighboring antiporter-like subunits in the membrane domain of complex I affect the proton transfer energetics. Our combined results suggest that opening of conserved Lys/Glu ion pairs within each antiporter-like subunit modulates the barrier for the lateral proton transfer reactions. Our work provides a mechanistic suggestion for key coupling effects in the long-range force propagation process of complex I.

Keywords

Bioenergetics; Proton transfer; NADH:ubiquinone oxidoreductase; Enzyme dynamics

1 Introduction

The respiratory complex I (NADH:ubiquinone oxidoreductase) is a redox-driven proton pump that serves as an initial electron entry point in prokaryotic and eukaryotic respiratory chains [1–4]. By reducing quinone (Q) to quinol (QH₂), complex I transports four protons across a biological membrane [1,5,6] and establishes a proton motive force (*pmf*) that is employed for active transport and synthesis of adenosine triphosphate (ATP) [7,8]. Complex I is by far the largest and most intricate member of the respiratory chain, and despite recently resolved structures [9–12], the molecular mechanism by which it pumps protons still remains unclear.

Complex I is a 0.5–1 MDa L-shaped enzyme that comprises up to 45 subunits in eukaryotes [13], and is organized into a hydrophilic domain and a membrane domain. The electron

^{*}Corresponding author. ville.kaila@ch.tum.de (V.R.I. Kaila).

Transparency document

The [Transparency document](#) associated with this article can be found in online version.

transfer process takes place in the ca. 100 Å long hydrophilic domain, whereas the 200 Å long membrane domain is responsible for the proton pumping function (Fig. 1). The 14 conserved core subunits of the enzyme constitute the machinery needed to catalyze the long-range proton-coupled electron transfer (PCET) process. The remaining 31 supernumerary subunits in the eukaryotic enzyme are organized around the core subunits [14–16] and are possibly involved in the regulation of enzyme functions, e.g., by the *active-to-deactive* transition [11,12,17–20], which modulates complex I activity.

The electron transport process is initiated by the oxidation of nicotinamide adenine dinucleotide (NADH), which transfers its two electrons via a non-covalently bound flavin mononucleotide (FMN) cofactor to a chain of 8–9 iron sulfur centers (ISC) and further to the Q-binding site, located ca. 30 Å above the membrane surface (Fig. 1) [9,21,22]. The electron transfer (eT) between NADH and the terminal N2 iron-sulfur center takes place on ca. 90 μs timescales [23,24], which is fast relative to the millisecond turnover of complex I [2], and thus not rate-limiting for the proton pumping process [2,25].

The Q pocket is located at the interface between the three subunits Nqo4, Nqo6, and Nqo8 (*T. thermophilus* nomenclature), and extends ca. 40 Å toward the membrane domain. There are to date no experimentally resolved structures of complex I with bound Q, but computational studies [26,27] suggest that Tyr₄-87 and His₄-38 stabilize the Q head-group and function as local proton donors in the Q-reduction process. These findings are also supported by site-directed mutagenesis studies [28,29]. The Q cavity has a non-uniform polarity, and it comprises a kink region with many polar and charged amino acids [9,30]. From this kink, a chain of conserved charged/polar residues extends in the middle of the membrane domain toward the terminal Nqo12 subunit [9,31].

Of the seven membrane domain subunits, three antiporter-like subunits, Nqo12, Nqo13, and Nqo14 are evolutionary related to each other and to multi-resistance and pH adaptation (Mrp) Na⁺/H⁺ antiporters. The antiporter-like subunits share an internal pseudo-symmetry, with two trans-membrane (TM) helix bundles, TM4-8 and TM9-13, that contain a broken-helix element. A similar five-helical bundle, TM2-6, is also present in the Nqo8 subunits, and it comprises a part of the Q channel. The proton pumping is likely to occur in the Nqo12, Nqo13, and Nqo14 subunits, pumping one proton each. The location of the fourth proton pathway is still under debate, but a possible location is the region between Nqo8 and Nqo11 [9,10]. Recent simulations [32–34] show that the proton channels are likely to form at the broken-helix segment, similar as in other transporters [35,36].

It is possible to identify conserved repeated residue motifs in each antiporter-like subunit. These include a Lys/Glu ion pair (Arg/Glu in Nqo12), a central Lys residue, one or more bridging His residues, and a terminal charged Lys or Glu residue (Fig. 1, *inset*). Site-directed mutagenesis experiments [37–42] and molecular simulations suggest that these residues are crucial for the proton pumping activity. Moreover, the Q reduction activity is also affected by mutations of these residues, suggesting that the electron and proton transfer processes are tightly coupled in complex I. Importantly, to achieve such tight coupling between the Q reaction and the terminal proton transfer in Nqo12, the “Q-reduction signal” needs to propagate through the complete membrane domain.

Biochemical, structural, and computational studies have probed possible proton pumping mechanisms ([25,33,42–46], cf. [44] and refs. therein). Although the overall pumping process takes place on milli-seconds timescales, individual transitions that couple to the pumping process may take place on much shorter timescales once a rate-limiting step has been overcome. Therefore, relaxation of such “non-equilibrium” state created here, e.g., by protonation changes, can be employed to obtain mechanistic information of rare events using molecular dynamics simulations that are shorter than the overall turnover timescale.

Recently, we suggested a molecular mechanism where conformational changes in the Lys/Glu ion pairs are involved in the long-range force propagation process and transmit the signal between neighboring antiporter-like subunits. This mechanism involves sequential Lys/Glu ion-pair dissociation and lateral proton transfer processes, propagating the signal from Nqo14 to Nqo12. We found that the energetics of ion-pair dissociations depends on the protonation state of the central Lys residues, making also the reverse effect possible, i.e., that the ion-pair dynamics modulate the pK_a of the neighboring amino acids. The protonic connectivity to the two membrane sides (N- and P-side) was further suggested to be regulated by the hydration state of *input* and *output* channels, which in turn is controlled by the state of buried charged residues. The water channels “*open*” and “*close*” on the sub- μ s timescale, which may provide a rate-limiting element in the proton pumping process. It was suggested that the proton N-side input and P-side output channels are located at symmetry-related positions. More specifically, the channels form at the interface between subunits and the 5-TM helices bundles, sharing the same symmetry and connecting the buried central Lys and terminal charged residues within each subunit to the N- and P-sides of the membrane [33]. The lateral proton transfer takes place between the central Lys residue and the charged residue facing the subsequent subunit. Each of these events triggers the following process and propagates across the complete ca. 200 Å membrane domain. We also suggested based on thermodynamic considerations [46] that the proton pumping process involves a “*backwave*” that couples to proton release across the membrane.

To study the energetics and dynamics of this coupling principle, we perform here classical molecular dynamics (MD) simulations in combination with quantum chemical density functional theory (DFT) calculations on the experimentally resolved X-ray structure of complex I from *Thermus thermophilus*. Our data suggest how the *inter*-subunit contacts are established and how these interactions could modulate the proton transfer energetics.

2 Models and methods

2.1 Classical molecular dynamics

The X-ray structure of *T. thermophilus* complex I [9] was embedded in a POPC membrane and solvated with TIP3P water, and the system was neutralized with a ca. 100 mM NaCl concentration. Ubiquinone (Q₁₀) was modeled in the Q-cavity, which was identified using the HOLE [47] software, and the Q headgroup was placed between His₄-38 and Tyr₄-87 of the Nqo4 subunit. The system comprised ca. 830,000 atoms. A constant temperature of 310 K and pressure of 1 bar were modeled in an *NPT* ensemble, and long-range electrostatics were treated by the Particle Mesh Ewald (PME) method [48]. The simulations were performed using NAMD2 [49] and the CHARMM27 force field [50,51] using a 2 fs

integration timestep. Force field parameters for the cofactors were derived from density functional theory (DFT/B3LYP/def2-TZVP) calculations. pK_a values were estimated using Poisson-Boltzmann (PB) continuum electrostatic calculations and performed using the Adaptive PB solver (APBS) [52], by performing the Monte Carlo sampling of the 2^N possible protonation states with Karlsberg+ [53]. The system was described by explicit partial atomic charges embedded in an inhomogeneous medium with an $\epsilon = 4$, and bulk water by a homogeneous medium with $\epsilon = 80$. Part of the simulation data were also employed in Ref. [33] and are reported in Table S1. Principal component analysis (PCA) [54,55] of the MD data was performed using the position of the C α atoms of subunits during 200–600 ns of dynamics (simulations 2 and 4) after 400 ns of simulation. The PCA and related analyses were performed with ProDy [56].

2.2 Quantum chemical density functional theory models

Quantum chemical DFT models consisting of the Lys₁₃-235, His₁₃-292 and Glu₁₃-377 residues of Nqo13 and Lys₁₄-216, His₁₄-265 and Lys₁₄-345 residues of Nqo14, with three intervening water molecules in each case, were constructed based on 100 ns relaxed MD simulations. The amino acid residues were cut at the C β (for His and Glu) or C δ (for Lys) positions, which were fixed during structure optimization at the B3LYP-D3/def2-SVP level [57–60]. The protein environment was treated as a polarizable medium with $\epsilon = 4$ using the conductor-like screening model (COSMO) [61]. Transition states were also optimized at the same level of theory. Electronic energies were computed at B3LYP-D3/def2-TZVP/ $\epsilon = 4$ level with zero-point vibrational (ZPE) energy corrections obtained at B3LYP-D3/def2-SVP/ $\epsilon = 4$ level. To study the effect of the Lys₁₃-204/Lys₁₄-186, we added a Lys α -amino group at 10.5 Å from the Lys₁₃-235/Lys₁₄-216. All calculations were performed with TURBOMOLE v 6.6 [62].

3 Results and discussion

3.1 Inter-subunit contacts affect intra-subunit residue conformations

Starting from the crystal structure of complex I from *Thermus thermophilus*, we performed ca. 3 μ s classical molecular dynamics (MD) simulations with the central polar residues modeled in both their protonated and deprotonated forms (Table S1). In the MD simulations, we find that the Lys/Arg-Glu ion pairs in each antiporter-like subunit form transient contacts with neighboring subunits that are stabilized by interactions with oppositely charged residues at their interface (Fig. 2). For each of the three interfaces Nqo11/Nqo14, Nqo13/Nqo14, and Nqo12/Nqo13, we observe a qualitatively similar behavior, with the key residues showing a two-state conformational switching behavior, which could be important for the signal propagation in the membrane domain of complex I.

We find that the Nqo13/Nqo14 interface has the clearest switching behavior (Fig. 3A). The MD simulations suggest that Glu₁₃-123 can form both an *intra*-subunit salt-bridge with Lys₁₃-204 and an *inter*-subunit contact with Lys₁₄-345 upon conformational switching (Fig. 2A, Fig. 3A). This switching is coupled with a decrease in the distance between Lys₁₃-204 and the central Lys₁₃-235 (Fig. 3A, *upper panel*), which could function as a primary proton donor in the pumping process [33], as also supported by site-directed mutagenesis

experiments [41]. The distance distribution for the Lys₁₃-235/Lys₁₃-204 pair shows two major sidechain conformations (Fig. 2A). When either of the residues is modeled in the deprotonated state, we obtain a mean distance of ca. 10.5 Å, whereas when both residues are in their protonated (charged) states, the electrostatic repulsion increases their mean distance to ca. 14.0 Å (Fig. 3A, *lower panel*), showing that the ion-pair dynamics is tightly coupled to the protonation state of the residues (Fig. 3A). Interestingly, in the crystal structure of complex I from *Thermus thermophilus* (PDB ID: 4HEA), the Lys₁₃-204/Glu₁₃-123 ion pair has been refined in the dissociated state, with Glu₁₃-123 flipped toward the Nqo14 subunit.

Similar as for Nqo13/Nqo14, we also observe a conformational switching at the interface between Nqo14 and Nqo11 (Fig. 3B). However, in contrast to the Nqo13/Nqo14 interface where Glu₁₃-123 interacts with two oppositely charged residues, Glu₁₄-112 is surrounded by Lys₁₄-186 and two acidic residues, Glu₁₁-67 and Glu₁₁-32 (Fig. 2B). Here we observe two distinct conformations of Glu₁₁-67, which result in a ca. 7 Å distance to Lys₁₄-186 when it is modeled in a protonated state, and a ca. 3.2 Å distance when is modeled in a deprotonated state (Fig. 3B), forming a hydrogen-bonded contact. When deprotonated, Glu₁₁-67 faces away from Glu₁₁-32, possibly due to electrostatic repulsion. Similar as in Nqo13, this conformational change correlates with an increase in the Lys₁₄-186/Lys₁₄-216 distance (Fig. 3B). Lys₁₄-216 is likely to function as the proton donor in subunit Nqo14 [33,44].

We next analyzed the ion-pair dynamics at the Nqo12/Nqo13 interface, which is structurally different from the other antiporter-like subunits. The Nqo12/Nqo13 interface comprises two positively charged residues, Lys₁₂-216 and Arg₁₂-163, which are compensated by three negatively charged residues, Glu₁₃-377, Glu₁₂-132, and Asp₁₂-166 (Fig. 2C). Arg₁₂-163 has been suggested to replace a putative Na⁺-binding site in their evolutionary ancestral Na⁺-pumping Mrp transporters [4]. Our MD simulations suggests that Arg₁₂-163 can form a salt-bridge with the surrounding acidic residues. In addition to the two distinct conformational states observed for the other interfaces, we also observe a third intermediate state (Fig. 3C, *lower panel*), which could arise from simultaneous interaction with both its acidic neighbors at the same time. We find that the strong interaction between Arg₁₂-163 and Asp₁₂-166 is anti-correlated with the opening of the Glu₁₃-377/Arg₁₂-163 ion pair (Fig. 3C, *upper panel*).

In Nqo12, the distance between the putative proton donor, Lys₁₂-329, and residues Lys₁₂-216/Asp₁₂-166 at the *inter*-subunit interface is larger than 18 Å, making a direct electrostatic coupling between the two sites somewhat weaker, as compared to the interaction in the other subunits. However, the conserved His₁₂-241 of TM8, located in the same position as the central Lys in Nqo13 and Nqo14, could provide a link necessary to couple the ion-pair dynamics to the proton transfer process. The higher complexity in Nqo12 might be related to the fact that it is the terminal antiporter-like subunit, and the coupling might be weaker than for the other subunits [4] (however, cf. also [46]).

3.2 Channel hydration and coupling between subunits

We recently observed a connection between the protonation state of the central Lys residues and the opening/closing dynamics of the proton channels in the antiporter-like subunits [33]. Our MD simulations suggest that in Nqo13, the water connectivity next to the broken helix TM7a is established when Lys₁₃-235 is protonated, and is lost upon its deprotonation (Fig.

4A). The hydration state of the antiporter-like subunit is, interestingly, also coupled with subtle structural changes (Fig. 4A). We observe that upon deprotonation of the middle Lys, the hydration level of the channel next to the broken helix TM7a drops significantly (Fig. 4B). Only one water molecule, which interacts with the deprotonated Lys, remains close to the TM4-8 helix bundle, whereas the remaining channel water is pushed toward the N-side by His₁₃₋₂₁₁ and Leu₁₃₋₂₁₄, which move closer together to form a gating element. Both residues are located on the upper part of the broken helix (TM7) of the antiporter-like subunit. Communication between the two parts of the helix (TM7a and TM7b) could be mediated by Trp₁₃₋₂₁₃ in TM7a, as indicated by a hydrogen-bond between the tryptophan and the backbone of Leu₁₃₋₂₀₃ of the lower helix (TM7b). The tilt of TM7a relative to TM7b also changes significantly after deprotonation of Lys₁₃₋₂₃₅ (Fig. 4B), which also couples to a subtle shift in the π -kink of TM8 with Lys₁₃₋₂₃₅. These conformational changes lead to a decrease in the channel radius by ca. 2 Å measured from the distance between Leu₁₃₋₂₁₄ on TM7a and Lys₁₃₋₂₈₇ on TM8, and a decrease in mean channel hydration by ca. 50% (within 4 Å of the gate, Fig. 4B).

The MD simulations performed with different protonation states reveal possible effects driving the opening/closure of channels. To further probe global coupling effects, we performed a principal component analysis (PCA) that projects out global slow relaxing degrees of freedom. The dynamical correlation between the antiporter-like subunits, calculated based on the PCA correlation matrix on different trajectories, shows how the coupling of motions could depend on both the hydration level of the subunits and the protonation states of the buried residues. When the putative proton channels are hydrated, we observe a strong coupling between the subunits (Fig. 5A). However, upon dehydration of the water channels by deprotonation of the central Lys, the coupling between subunits weakens as indicated by a reduced correlation (Fig. 5B).

Although analysis of more intermediate states is needed to clarify details of the coupling between subunits, our data nevertheless indicate that the protonation state of conserved residues and channel hydration affect complex I dynamics. This suggests that not only the protein structure, but also the water molecules play an active role in the pumping process, by providing essential coupling elements that transmit the signal in addition to their role as “proton wires”.

3.3 Inter-subunit contacts modulate proton transfer energetics

To “push” the proton horizontally within the antiporter-like domains, complex I must invest energy by destabilizing the protonated middle Lys. As described above, this could be achieved by opening of the Lys/Glu ion pair, which is expected to result in a charge repulsion between Lys₁₃₋₂₀₄ and Lys₁₃₋₂₃₅ (in Nqo13), as also suggested by recent free energy simulations [33]. To qualitatively probe such coupling principles, we built quantum chemical model systems comprising the sidechains of residues Lys-His-Lys and Lys-His-Glu (proton donor – bridging residue – proton acceptor), bridging water molecules, and using a protonated Lys sidechain as “*triggering signal*” for the proton transfer process (Fig. 6). The structures were extracted from the classical MD simulations of complex I after ca. 100 ns. After DFT optimization of intermediate and transitions states, we studied the energetics of

the proton transfer reaction for this model system by probing the effect of a positive charge next to the proton donor, mimicking the charge of the unpaired Lys resulting from the flip of the interface salt-bridges to the neighboring subunit.

In subunit Nqo13 (Fig. 6A), our quantum chemical models suggest that proton transfer from Lys₁₃-235 to His₁₃-292 via one bridging water molecule (A1 to A3 in Fig. 6A) has an energy barrier of ca. 4 kcal mol⁻¹ and takes place via a hydronium-like transition state structure. The process is exergonic by ca. 5 kcal mol⁻¹. The effect of the un-compensated Lys₁₃-204 lowers this barrier by ca. 2 kcal mol⁻¹ and renders the reaction more exergonic by ca. 3 kcal mol⁻¹. The subsequent proton transfer from His₁₃-292 to Glu₁₃-377 via two water molecules (A3 to A5 in Fig. 6A) has a barrier of ca. 6 kcal mol⁻¹, with a transition state resembling a Zundel ion, and a reaction energy of ca. -14 kcal mol⁻¹. The exergonicity of this process is likely to be over-estimated due to the neutralization of an uncompensated negative Glu in a low dielectric environment. The presence of the unpaired Lys sidechain at 10.5 Å from Lys₁₃-235 stabilizes both the intermediate and final states (A3 to A5 in Fig. 6A) by ca. 3 kcal mol⁻¹, conserving the barrier of ca. 5 kcal mol⁻¹. In subunit Nqo14 (Fig. 6B), the energetics of the proton transfer from Lys₁₄-216 to His₁₄-292 (B1 to B3 in Fig. 6B) is similar as in the Nqo13 subunit model, with a barrier of ca. 5 kcal mol⁻¹ and an exergonicity of ca. 5 kcal mol⁻¹. We find that the charge of Lys₁₄-186 could stabilize this hydronium-ion transition state by ca. 2 kcal mol⁻¹, but it slightly destabilizes the protonated His₁₄-262 by ca. 1 kcal mol⁻¹. Proton transfer from His₁₄-262 to Lys₁₄-345 via two water molecules (B3 to B5 in Fig. 6B) has a relatively high energy barrier of ca. 15 kcal mol⁻¹ in the model system, and it is endergonic by ca. 7 kcal mol⁻¹, yielding a final state which is ca. 2 kcal mol⁻¹ higher in energy than the initial state. However, the charge of the uncompensated Lys lowers the barrier by ca. 4 kcal mol⁻¹ and makes the reaction more exergonic by ca. 4 kcal mol⁻¹, now being stabilized relative to the initial state by ca. 2 kcal mol⁻¹. The intermediates and transition states observed in our QM cluster models are consistent with the ones from QM/MM-models probed in our previous study [33].

Although the proton transfer model employed here is simple, it nevertheless captures qualitative features on how modulation of the proton transfer energetics could be achieved in complex I. The model also describes some of the essential features needed to create a tightly coupled proton pumping machinery. While here the cost to change the energetics of the system is given by the energy required to “create” a positive charge next to our proton transfer chain, the same process in the complete system would also include the free energy caused by the separation of the ion pair and creation of the “excess charge”. Free energy computations [33] estimate these effects as 3–4 kcal mol⁻¹ with a deprotonated central Lys and > 8 kcal mol⁻¹ when Lys₁₃-235 is modeled in a protonated state. The models thus support that the inter-subunit ion pairs could influence the lateral proton transfer reaction and coupling between subunits propagated.

4 Conclusions

Our molecular simulations presented here provide insight on how *inter*-subunit contacts can modulate the proton transfer processes in the antiporter-like subunits of complex I. The proton pumping in the membrane domain of complex I, involves proton transfer reactions

between the N-side bulk and buried titratable lysine residues, as well as horizontally across the membrane domain. Our simulations indicate that the energetics and kinetics of these proton transfer reactions are coupled to the charged state of a conserved ion pair within each antiporter-like subunit, and in turn, regulated by the charged state of the neighboring subunit. Our data indicate that Glu₁₃₋₁₂₃ in Nqo13, could act as a two-state conformational switch, by interaction with Lys₁₄₋₃₄₅ of Nqo14. The resulting uncompensated charge of Lys₁₃₋₂₀₄ could therefore lead to proton transfer to Glu₁₃₋₃₇₇. Quantum chemical model calculations of these processes further support that the conformational state of the Lys/Glu ion pair indeed strongly modulates the proton transfer energetics. Moreover, our principal component analysis of global dynamics in the membrane domain of complex I suggests that the ion-pair dynamics is also linked with channel hydration and *inter*-subunit couplings. We observe similar effects as described for Nqo13, also in the other antiporter-like subunits. Our combined results suggest that a combination of conformational and electrostatic switching provide an important functional principle to achieve an *action-at-a-distance* effect in complex I.

Supplementary Material

Refer to Web version on PubMed Central for supplementary material.

Acknowledgements

This work received funding from the European Research Council (ERC) under the European Union's Horizon 2020 research and innovation program/grant agreement 715311. The Leibniz-Rechenzentrum (LRZ), SuperMuc (projects: pr48de and pr27xu) provided computational resources.

References

- [1]. Wikström M. Two protons are pumped from the mitochondrial matrix per electron transferred between NADH and ubiquinone. *FEBS Lett.* 1984; 169(2):300–304. [PubMed: 6325245]
- [2]. Hirst J. Mitochondrial complex I. *Annu Rev Biochem.* 2013; 82(1):551–575. [PubMed: 23527692]
- [3]. Brandt U. Energy converting NADH: ubiquinone oxidoreductase (complex I). *Annu Rev Biochem.* 2006; 75(1):69–92. [PubMed: 16756485]
- [4]. Sazanov LA. A giant molecular proton pump: structure and mechanism of respiratory complex I. *Nat Rev Mol Cell Biol.* 2015; 16(6):375–388. [PubMed: 25991374]
- [5]. Jones AJY, Blaza JN, Varghese F, Hirst J. Respiratory complex I in *Bos taurus* and *Paracoccus denitrificans* pumps four protons across the membrane for every NADH oxidised. *J Biol Chem.* 2017; 292(12):4987–4995. [PubMed: 28174301]
- [6]. Galkin AS, Grivennikova VG, Vinogradov AD. H⁺/2e⁻ stoichiometry in NADH-quinone reductase reactions catalyzed by bovine heart submitochondrial particles. *FEBS Lett.* 1999; 451(2):157–161. [PubMed: 10371157]
- [7]. Mitchell P. Coupling of phosphorylation to electron and hydrogen transfer by a chemi-osmotic type of mechanism. *Nature.* 1961; 191(4784):144–148. [PubMed: 13771349]
- [8]. Yoshida M, Muneyoki E, Hisabori T. ATP synthase — a marvelous rotary engine of the cell. *Nat Rev Mol Cell Biol.* 2001; 2(9):669–677. [PubMed: 11533724]
- [9]. Baradaran R, Berrisford JM, Minhas GS, Sazanov LA. Crystal structure of the entire respiratory complex I. *Nature.* 2013; 494(7438):443–448. [PubMed: 23417064]
- [10]. Zickermann V, Wirth C, Nasiri H, Siegmund K, Schwalbe H, Hunte C, Brandt U. Mechanistic insight from the crystal structure of mitochondrial complex I. *Science.* 2015; 347(6217):44–49. [PubMed: 25554780]

- [11]. Zhu J, Vinothkumar KR, Hirst J. Structure of mammalian respiratory complex I. *Nature*. 2016; 536(7616):354–358. [PubMed: 27509854]
- [12]. Fiedorczuk K, Letts JA, Degliesposti G, Kaszuba K, Skehel M, Sazanov LA. Atomic structure of the entire mammalian mitochondrial complex I. *Nature*. 2016; 538(7625):406–410. [PubMed: 27595392]
- [13]. Carroll J, Fearnley IM, Skehel JM, Shannon RJ, Hirst J, Walker JE. Bovine complex I is a complex of 45 different subunits. *J Biol Chem*. 2006; 281(43):32724–32727. [PubMed: 16950771]
- [14]. Vinothkumar KR, Zhu J, Hirst J. Architecture of mammalian respiratory complex I. *Nature*. 2014; 515(7525):80–84. [PubMed: 25209663]
- [15]. Wirth C, Brandt U, Hunte C, Zickermann V. Structure and function of mitochondrial complex I. *Biochim Biophys Acta*. 2016; 1857(7):902–914. [PubMed: 26921811]
- [16]. Kmita K, Zickermann V. Accessory subunits of mitochondrial complex I. *Biochem Soc Trans*. 2013; 41(5):1272–1279. [PubMed: 24059519]
- [17]. Maklashina E, Kotlyar AB, Cecchini G. Active/de-active transition of respiratory complex I in bacteria, fungi and animals. *Biochim Biophys Acta*. 2003; 1606(1):95–103. [PubMed: 14507430]
- [18]. Vinogradov AD. Catalytic properties of the mitochondrial NADH-ubiquinone oxidoreductase (complex I) and the pseudo-reversible active/inactive enzyme transition. *Biochim Biophys Acta*. 1998; 1364(2):169–185. [PubMed: 9593879]
- [19]. Dröse S, Stepanova A, Galkin A. Ischemic A/D transition of mitochondrial complex I and its role in ROS generation. *Biochim Biophys Acta*. 2016; 1857(7):946–957. [PubMed: 26777588]
- [20]. Di Luca A, Kaila VRI. Global collective motions in the mammalian and bacterial respiratory complex I. *Biochim Biophys Acta*. 2018; 1859(5):326–332.
- [21]. Hunte C, Zickermann V, Brandt U. Functional modules and structural basis of conformational coupling in mitochondrial complex I. *Science*. 2010; 329(5990):448–451. [PubMed: 20595580]
- [22]. Sazanov LA, Hinchliffe P. Structure of the hydrophilic domain of respiratory complex I from *Thermus thermophilus*. *Science*. 2006; 311(5766):1430–1536. [PubMed: 16469879]
- [23]. Verkhovskaya ML, Belevich N, Euro L, Wikström M. Real-time electron transfer in respiratory complex I. *Proc Natl Acad Sci U S A*. 2008; 105(10):3763–3767. [PubMed: 18316732]
- [24]. De Vries S, Dörner K, Stramprecht MJF, Friedrich T. Electron tunneling rates in respiratory complex I are tuned for efficient energy conversion. *Angew Chem Int Ed*. 2015; 54:2844–2848.
- [25]. Verkhovskaya M, Bloch DA. Energy-converting respiratory complex I: on the way to the molecular mechanism of the proton-pump. *Int J Biochem Cell Biol*. 2013; 45(2):491–511. [PubMed: 22982742]
- [26]. Sharma V, Belevich G, Gamiz-Hernandez AP, Róg T, Vattulainen I, Verkhovskaya ML, Wikström M, Hummer G, Kaila VRI. Redox-induced activation of the proton pump in the respiratory complex I. *Proc Natl Acad Sci U S A*. 2015; 112(37):11571–11576. [PubMed: 26330610]
- [27]. Gamiz-Hernandez AP, Jussupow A, Johansson MP, Kaila VRI. Terminal electron-proton transfer dynamics in the quinone reduction of respiratory complex I. *J Am Chem Soc*. 2017; 139(45):16282–16288. [PubMed: 29017321]
- [28]. Tocilescu MA, Fendel U, Zwicker K, Dröse S, Kerscher S, Brandt U. The role of a conserved tyrosine in the 49-kDa subunit of complex I for ubiquinone binding and reduction. *Biochim Biophys Acta*. 2010; 1797(22):625–632. [PubMed: 20117074]
- [29]. Sinha PK, Castro-Guerrero N, Patki G, Sato M, Torres-Bacete J, Sinha S, Miyoshi H, Mitsuno-Yagi A, Yagi T. Conserved amino acid residues of the NuoD segment important for structure and function of *Escherichia coli* NDH-1 (complex I). *Biochemistry*. 2015; 54(3):753–764. [PubMed: 25545070]
- [30]. Fedor JG, Jones AJY, Di Luca A, Kaila VRI, Hirst J. Correlating kinetic and structural data on ubiquinone binding and reduction by respiratory complex I. *Proc Natl Acad Sci U S A*. 2017; 114(48):12737–12742. [PubMed: 29133414]
- [31]. Efremov RG, Sazanov LA. Structure of the membrane domain of the respiratory complex I. *Nature*. 2011; 465(7297):414–420.

- [32]. Kaila VRI, Wikström M, Hummer G. Electrostatics, hydration and proton transfer dynamics in the membrane domain of respiratory complex I. *Proc Natl Acad Sci U S A*. 2014; 111(19):6988–6993. [PubMed: 24778264]
- [33]. Di Luca A, Gamiz-Hernandez AP, Kaila VRI. Symmetry-related proton transfer pathways in respiratory complex I. *Proc Natl Acad Sci U S A*. 2017; 114(31):E6314–E6321. [PubMed: 28716925]
- [34]. Haapanen O, Sharma V. Role of water and protein dynamics in proton pumping by respiratory complex I. *Sci Rep*. 2017; 7(7747):1–12. [PubMed: 28127051]
- [35]. Screpanti E, Hunte C. Discontinuous membrane helices in transport proteins and their correlation with function. *J Struct Biol*. 2007; 159:261–267. [PubMed: 17350860]
- [36]. Forrest LR, et al. Mechanism for alternating access in neurotransmitter transporters. *Proc Natl Acad Sci U S A*. 2008; 105:10338–10343. [PubMed: 18647834]
- [37]. Torres-Bacete J, Nakamaru-Ogiso E, Matsuno-Yagi A, Yagi T. Characterization of the NuoM (ND4) subunit in *Escherichia coli* NDH-1: conserved charged residues essential for energy-coupled activities. *J Biol Chem*. 2007; 282(51):36914–36922. [PubMed: 17977822]
- [38]. Kao MC, Di Bernardo S, Perego M, Nakamaru-Ogiso E, Matsuno-Yagi A, Yagi T. Functional role of four conserved charged residues on the membrane domain subunit NuoA of the proton-translocating NADH-quinone oxidoreductase from *Escherichia coli*. *J Biol Chem*. 2004; 279(31):32360–32366. [PubMed: 15175326]
- [39]. Torres-Bacete J, Sinha PK, Castro-Guerrero N, Matsuno-Yagi A, Yagi T. Features of subunit NuoM (ND4) subunit in *Escherichia coli* NDH-1: topology and implication of conserved Glu144 for coupling site 1. *J Biol Chem*. 2009; 284(48):33062–33069. [PubMed: 19815558]
- [40]. Nakamaru-Ogiso E, Kao MC, Chen H, Sinha SC, Yagi T, Ohnishi T. The membrane subunit NuoL (ND5) is involved in the indirect proton pumping mechanism of *Escherichia coli* Complex I. *J Biol Chem*. 2010; 285(50):39070–39078. [PubMed: 20826797]
- [41]. Michel J, Deleon-Rangel J, Zhu S, Van Ree K, Vik SB. Mutagenesis of the L, M, and N subunits of complex I from *Escherichia coli* indicates a common role in function. *PLoS One*. 2011; 6(2):e17420. [PubMed: 21387012]
- [42]. Euro L, Belevich G, Verkhovskiy MI, Wikström M, Verkhovskaya M. Conserved lysine residues of the membrane subunit NuoM are involved in energy conversion by the proton-pumping NADH:ubiquinone oxidoreductase (complex I). *Biochim Biophys Acta*. 2008; 1777(9):1166–1172. [PubMed: 18590697]
- [43]. Wikström M, Hummer G. Stoichiometry of the proton translocation by respiratory complex I and its mechanistic implications. *Proc Natl Acad Sci U S A*. 2012; 109(12):4431–4436. [PubMed: 22392981]
- [44]. Wikström M, Sharma V, Kaila VRI, Hosler JP, Hummer G. New perspectives on the proton pumping in cellular respiration. *Chem Rev*. 2015; 115(5):2196–2221. [PubMed: 25694135]
- [45]. Brandt U. A two-state stabilization-change mechanism for proton-pumping complex I. *Biochim Biophys Acta*. 2011; 1807(10):1364–1369. [PubMed: 21565159]
- [46]. Kaila VRI. Long-range proton-coupled electron transfer in biological energy conversion: towards mechanistic understanding of respiratory complex I. *J Roy Soc Interfaces*. 2018; 141(15)
- [47]. Smart OS, Neduveilil JG, Wang X, Wallace BA, Sansom MSP. HOLE: a program for the analysis of the pore dimensions of ion channel structural models. *J Mol Graph*. 1996; 14(6):354–360. [PubMed: 9195488]
- [48]. Darden T, York D, Pedersen L. Particle mesh Ewald: an $N\log(N)$ method for Ewald sums in large systems. *J Chem Phys*. 1993; 98(12):10089–10092.
- [49]. Phillips JC, Braun R, Wang W, Gumbart J, Tajkhorshid E, Villa E, Chipot C, Skeel RD, Laxmikant K, Schulten K. Scalable molecular dynamics with NAMD. *J Comput Chem*. 2005; 26(16):1781–1802. [PubMed: 16222654]
- [50]. MacKerell AD, Bashford D, Bellott M, Dunbrack RL, Evanseck JD, Field MJ, Fischer S, Gao J, Guo H, Ha S, Joseph-McCarthy D, et al. All atom empirical potential for molecular modeling and dynamics studies of proteins. *J Phys Chem B*. 1998; 102(18):3586–3616. [PubMed: 24889800]

- [51]. Klauda JB, Venable RM, Freites JA, O'Connor JW, Tobias DJ, Mondragon-Ramirez C, Vorobyov I, MacKerell AD Jr, Pastor RW. Update of the CHARMM all-atom additive force field for lipids: validation of six lipid types. *J Phys Chem B*. 2010; 114(23):7830–7843. [PubMed: 20496934]
- [52]. Baker NA, Sept D, Joseph S, Holst MJ, McCammon JA. Electrostatic of nano-systems: application to microtubules and the ribosome. *Proc Natl Acad Sci U S A*. 2001; 98:10037–10041. [PubMed: 11517324]
- [53]. Kieseritzky G, Knapp EW. Optimizing pKa computation in proteins with pH adapted conformations. *Proteins*. 2008; 71(3):1335–1348. [PubMed: 18058906]
- [54]. Bahar I, Lezon TR, Bakan A, Shrivastava IH. Normal mode analysis of biomolecular structures: functional mechanisms of membrane proteins. *Chem Rev*. 2010; 110(3):1463–1497. [PubMed: 19785456]
- [55]. Van Wynsberghe AW, Cui Q. Interpreting correlated motions using normal mode analysis. *Structure*. 2006; 14(1):1647–1653. [PubMed: 17098190]
- [56]. Bakan A, Meireles LM, Bahar I. Prody: protein dynamics inferred from theory and experiments. *Bioinformatics*. 2011; 27(11):1575–1577. [PubMed: 21471012]
- [57]. Becke AD. Density-functional thermochemistry. III. The role of exact-exchange. *J Chem Phys*. 1993; 98(7):5648–5652.
- [58]. Lee C, Yang W, Parr RG. Development of the Colle-Salvetti correlation-energy formula into a functional of the electron density. *Phys Rev B Condens Matter*. 1988; 37(2):785–789. [PubMed: 9944570]
- [59]. Weigend F, Ahlrichs R. Balanced basis sets of split valence, triple zeta valence and quadruple zeta valence quality for H to Rn: design and assessment of accuracy. *Phys Chem Chem Phys*. 2005; 7(18):3297–3305. [PubMed: 16240044]
- [60]. Grimme S, Antony J, Ehrlich S, Krieg HJ. A consistent and accurate ab initio parametrization of density functional dispersion correction (DFT-D) for the 94 elements H-Pu. *J Chem Phys*. 2010; 132(15)
- [61]. Klamt A, Schüürmann. COSMO: a new approach to dielectric screening in solvents with explicit expressions for the screening energy and its gradient. *J Chem Soc Perkin Trans*. 1993; 2:799–805.
- [62]. Ahlrichs R, Bär M, Häser M, Horn H, Kölmel C. Electronic structure calculations on workstation computers: the program system Turbomole. *Chem Phys Lett*. 1989; 162(3):165–169.

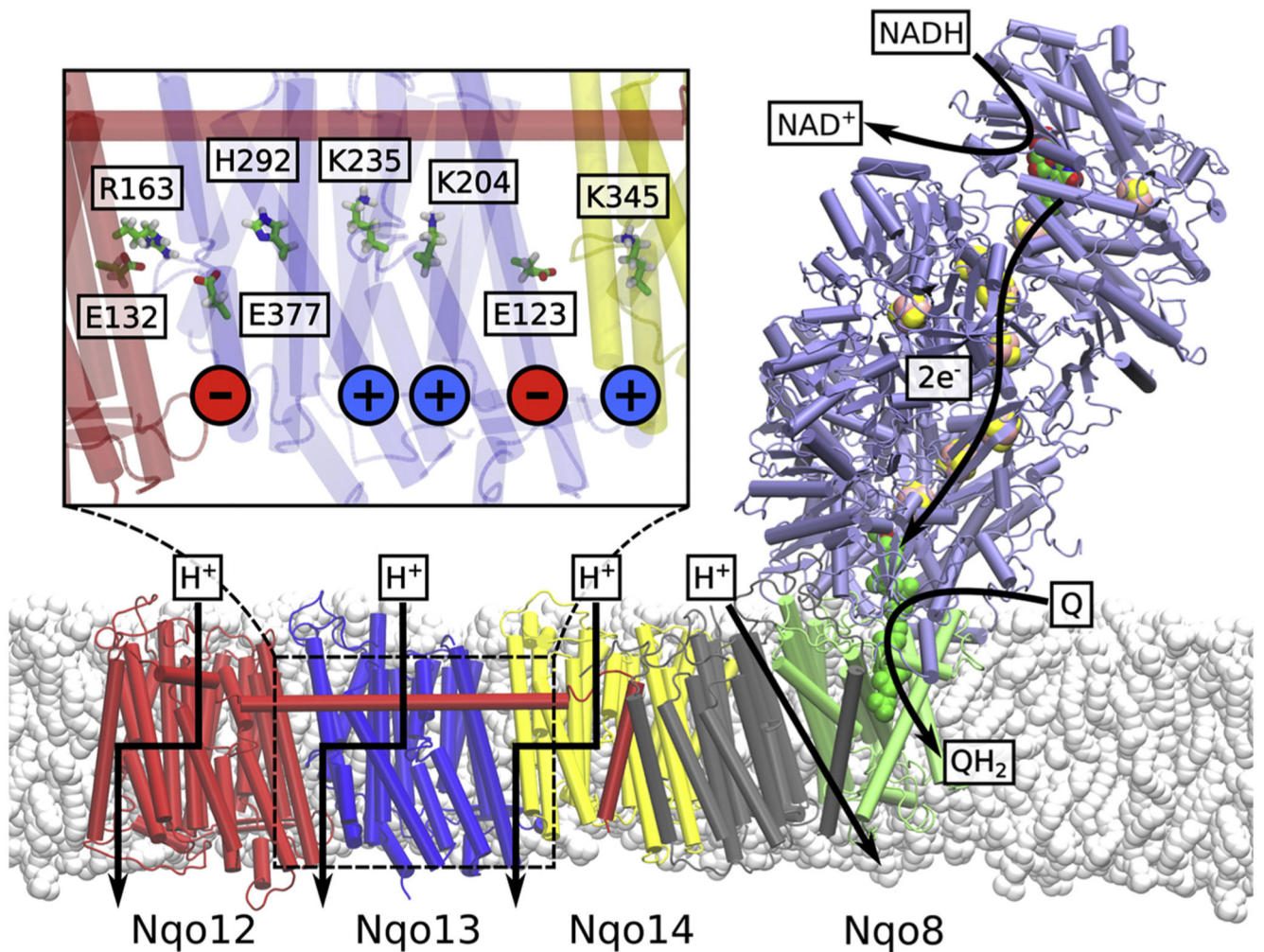
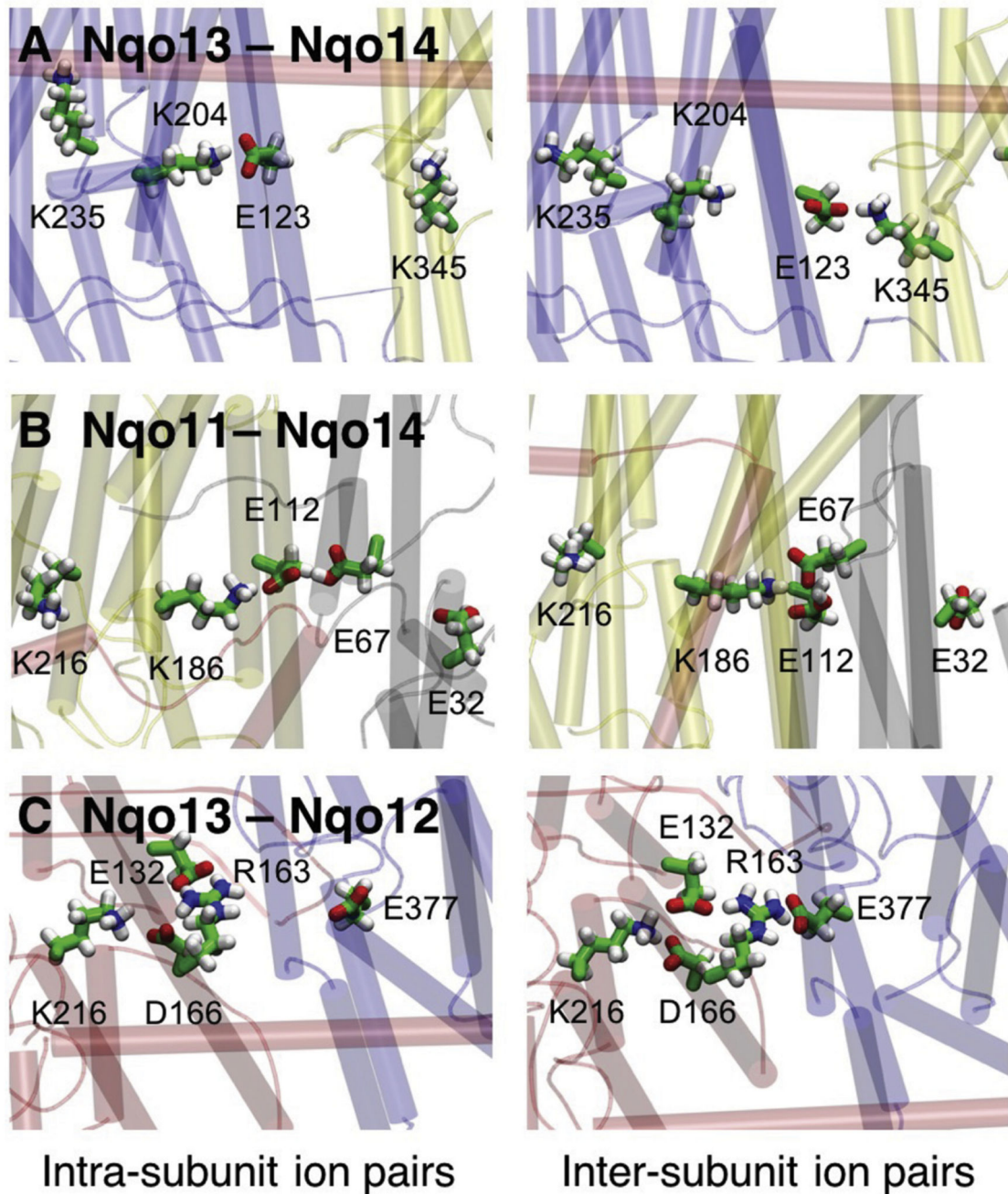


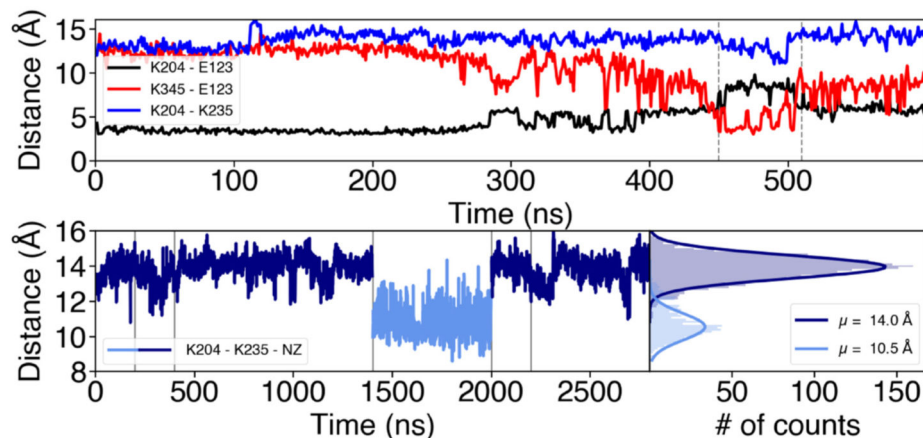
Fig. 1.

Structure of the bacterial complex I from *T. thermophilus* (PDB ID: 4HEA). Electron transfer takes place in the hydrophilic domain (in purple) between NADH and Q. Energy released from the Q reduction process is employed to transfer four protons across the membrane. The antiporter-like subunits Nqo12 (in red), Nqo13 (in blue) and Nqo14 (in yellow) are likely to transfer one proton each, whereas the location of the fourth proton pathway is still not fully clear (but cf. [33,34]). *Inset*: Chain of conserved charged and polar residues in Nqo13. From right to left: terminal charged residue of Nqo14, the Glu/Lys ion pair, the central Lys, the bridging His, the terminal charged residue of Nqo13 (Glu), and the interface to Nqo12.

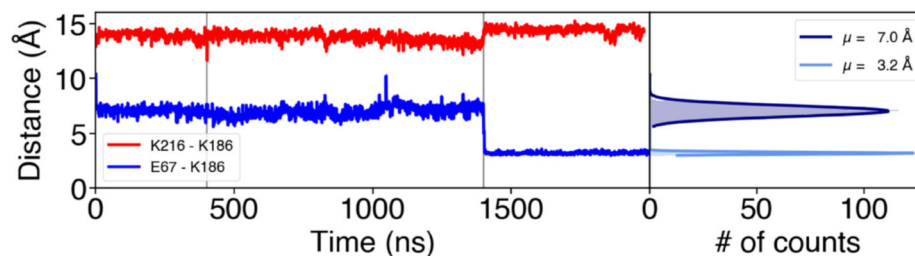
**Fig. 2.**

Structure of the antiporter-like subunit interfaces in the membrane domain of complex I. The figure shows A) the Nqo13-Nqo14 interface, B) the Nqo11-Nqo14 interface, and C) the Nqo13-Nqo12 interface. Ion pairs between conserved charged residues form alternating contacts within the same and neighboring subunits, with snapshots of *intra*-subunit contacts (to the left) and *inter*-subunit contacts (to the right).

A Nqo13 - Nqo14



B Nqo11 - Nqo14



C Nqo12 - Nqo13

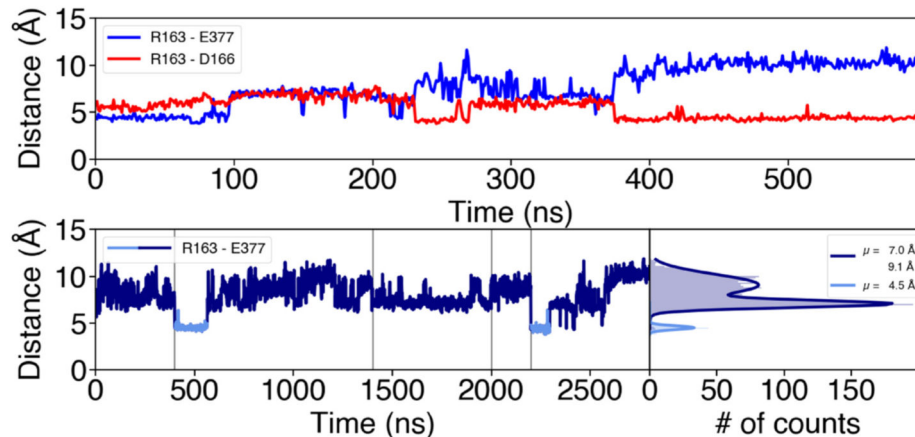
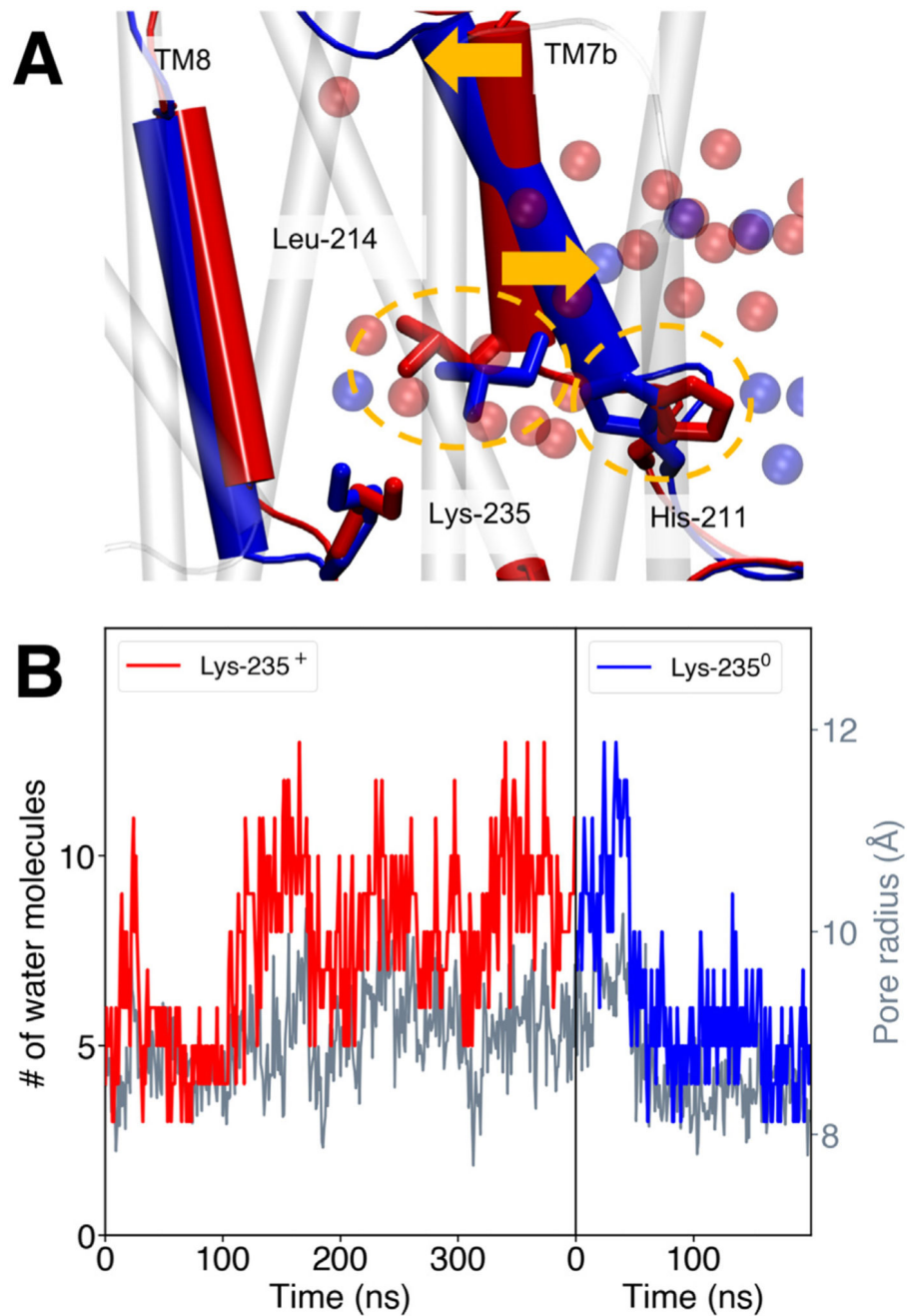


Fig. 3.

Ion-pair dynamics at the subunit interfaces in the membrane domain of complex I. A) The Nqo13 – Nqo14 interface. *Upper panel:* Distances of the Lys₁₃-204/Glu₁₃-123 ion pair (in black), the Lys₁₄-345/Glu₁₃-123 ion pair (in red) during 0.6 μ s of MD simulation (simulation 5). The flip of the ion pair correlates with a decrease in the Lys₁₃-204/Lys₁₃-235 distance (in blue). *Lower panel:* Lys₁₃-235/Lys₁₃-204 distances and their distribution during 2.8 μ s of dynamics (simulations 1 to 5). The dark blue curve represents a ‘repulsive’ regime where both residues are positively charged, whereas deprotonation of Lys₁₃-204 leads to

sampling of shorter distances (light blue curve). Vertical grey lines indicate boundaries between separate simulations. B) The Nqo11 – Nqo14 interface. Distances of the Glu₁₁₋₆₇/Lys₁₄₋₁₈₆ (in blue) and Lys₁₄₋₁₈₆/Lys₁₄₋₂₁₆ (in red) ion pairs during 2 μ s MD simulations (simulations 1, 2, 5) and the distribution of the distances between Glu₁₁₋₆₇/Lys₁₄₋₁₈₆ during the MD simulations. Upon deprotonation of Glu₁₁₋₆₇ at 1.4 μ s, the inter-subunit contact forms, which correlates with an increase in the Lys₁₄₋₁₈₆/Lys₁₄₋₂₁₆ distance. Deprotonation of Glu₁₁₋₆₇ leads to formation of contact with Lys₁₄₋₁₈₆. C) The Nqo12 – Nqo13 interface. *Upper panel:* Distances of the Arg₁₂₋₁₆₃/Glu₁₃₋₃₇₇ (in blue) and the Arg₁₂₋₁₆₃/Asp₁₂₋₁₆₆ (in red) ion pairs during 0.6 μ s of MD simulation (simulation 5). Arg₁₂₋₁₆₃ forms *inter-* and *intra-*subunit salt-bridges. *Lower panel:* Distances between Arg₁₂₋₁₆₃/Glu₁₃₋₃₇₇ during 2.8 μ s of simulation (simulations 1 to 5) and their respective distribution. *Intra-*subunit and intermediate states are drawn in dark-blue and the *inter-*subunit state in light blue. Vertical grey lines indicate boundaries between separate simulations.

**Fig. 4.**

A) Conformational changes associated with deprotonation of the central Lys₁₃-235 in subunit Nqo13 in the membrane domain of complex I. When Lys₁₃-235 is simulated in a protonated state (red, simulation 2) the gate formed by the sidechains of Leu₁₃-214 and His₁₃-211 (yellow circles) is open, whereas the gate closes when Lys₁₃-235 is modeled in a deprotonated state (blue, simulation 4), inducing dehydration of the channel. The opening/closing is coupled to a structural tilting of the TM7b broken helix (yellow arrows). B) The channel hydration state (in red and blue) and channel radius (in grey) for subunit Nqo13

with Lys₁₃-235 modeled the protonated (simulation 2, red) and deprotonated states (simulation 4, blue), respectively. The hydration state is measured as the number of water molecules within 4 Å around the Leu₁₃-214/His₁₃-211 gate. The pore radius is measured as distance between Leu₁₃-214 (TM7a) and Lys₁₃-287 (TM8). The mean hydration changes from four water molecules to eight water molecules during channel opening.

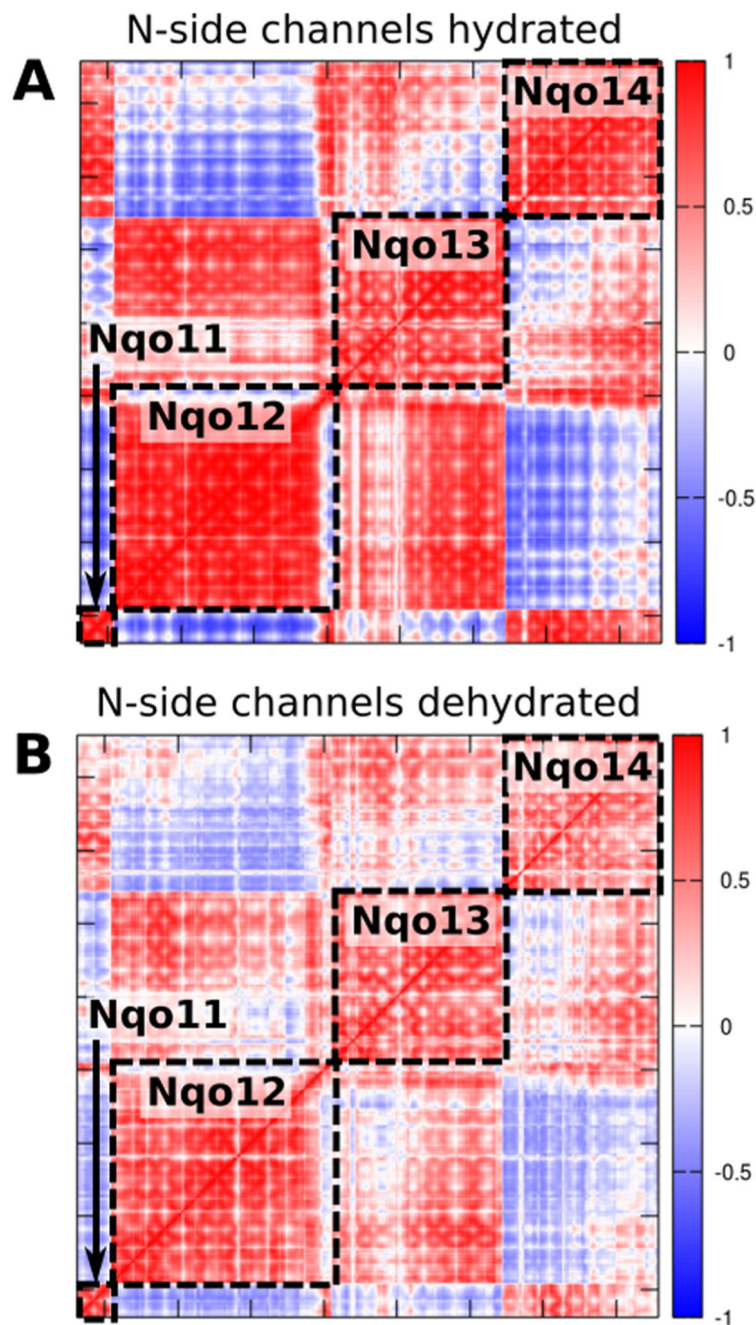


Fig. 5. Correlation matrices of the membrane domain of complex I obtained from principal component (PC) analysis of the MD simulation data (simulations 2 and 4, Table S1). Correlation of PCs A) with open channels between the N-side bulk water and central Lys residues, B) upon deprotonation of the central Lys residues and closure of the N-side channels. Neutralization and/or dehydration of the subunits cause a decreased coupling between subunits. The colors refer to the inter-residue correlation from 1 (directly correlated), to -1 (anti-correlated).

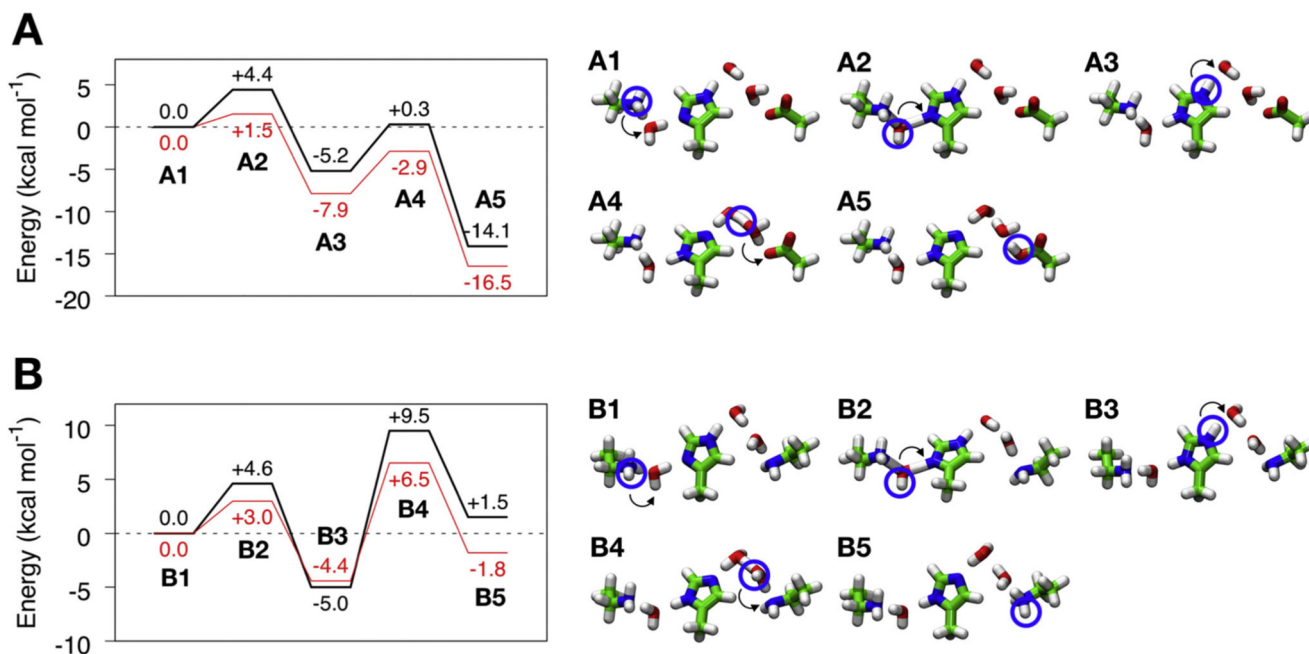


Fig. 6.

Effect of dissociation of the “Glu-Lys” ion pair on proton transfer energetics in minimal quantum chemical models of the proton pathway in A) Nqo13 and B) Nqo14. Energy profiles (in kcal mol^{-1}) are shown to the left and the corresponding structures of optimized intermediates and transition states are drawn on the right. Profiles in red show the effect of adding a polarizing Lys⁺, that forms upon dissociation of the Lys/Glu ion pair. The energetics were estimated at B3LYP/def2-TZVP/e = 4 level with zero-point energy (ZPE) corrections calculated at the B3LYP/def2-SVP level.